ISSN 0027-1349, Moscow University Physics Bulletin, 2010, Vol. 65, No. 3, pp. 195–202. © Allerton Press, Inc., 2010.
Original Russian Text © V.I. Galkin, T.A. Dzhatdoev, 2010, published in Vestnik Moskovskogo Universiteta. Fizika, 2010, No. 3, pp. 37–43.

On the Sensitivity of the Spatial–Angular Distribution of the Cherenkov Light in Extensive Air Showers to the Mass Composition of Primary Cosmic Rays with Energies of 10^{15}–10^{16} eV

V. I. Galkin[a, b] and T. A. Dzhatdoev[a, b]

[a] *Chair of Space Physics, Faculty of Physics, Moscow State University, Moscow, 119991 Russia*
[b] *Skobel'tsyn Institute of Nuclear Physics, Moscow State University, Moscow, 119991 Russia*
e-mail: v_i_galkin@rambler.ru, timur1606@rambler.ru

Received January 15, 2010; accepted February 06, 2010

Abstract—This paper analyses the possibility of separating distinct groups of nuclei of primary cosmic rays with energies of 10^{15}–10^{16} eV from the data on the spatial-angular distribution of Cherenkov light in extensive air showers. The paper shows that using an array of a few (3–4) telescopes with a moderately sized angular cell ~0.5° placed at a distance ~100 m from one another, one can achieve almost complete separation of the showers initiated by these nuclei (the Bayesian classification error is a few percentage points for the case of separating primary protons and nitrogen nuclei). The authors propose new parameters of the angular Cherenkov image that can greatly enhance the separability of the shower classes as compared to the approach based on the traditional parameters.

Key words: primary cosmic rays (PCR), mass composition, extensive air showers (EAS).
DOI: 10.3103/S0027134910030082

INTRODUCTION

One of the main problems of cosmic-ray physics is investigation of the mass composition of primary cosmic rays (PCR). The mass composition of cosmic rays in the "knee" region of the primary spectrum ($E_0 \sim 10^{15}$–10^{16} eV) is directly connected with the problems of their origin, acceleration, and propagation in the Galaxy.

At present, PCR can be measured directly with satellite and stratospheric balloon detectors up to primary energies of ~10^{14} eV. At higher energies, one usually applies indirect methods. In the latter case, the primary particle parameters are estimated by the characteristics of nuclear–electromagnetic cascade the particle initiates in the atmosphere, which is referred to as an extensive air shower (EAS).

Almost 20 years of the mass composition measurements by indirect methods have not yet given a definite answer: the simplest integral characteristic "the average mass number," is known with an accuracy of several mass units, and, in the knee region, the value range reaches an order of magnitude (Fig. 1). Of particular importance is the existence of serious discrepancies between measurements conducted by similar methods. For example, the results produced by KASKADE and EAS-TOP for $N_e - N_\mu$-correlations [2, 3] and those by BASJE, CASA-BLANCA, HEGRA-AIROBICC and TUNKA-25 [1, 4–6] for the lateral distribution of the Cherenkov light (CL) in EAS are seriously different.

We think that this can be explained by the following reasons:

—overestimation of the sensitivity of the applied methods to the mass of the primary particle and their stability to the measurement errors;

—the fact that the procedure for estimating the mass number A in the methods using the EAS Cherenkov light includes an intermediate stage, i.e., the transition from the measured parameters to $X_{\max}$, the depth of the shower maximum in the atmosphere. This shower parameter correlates with A but does not contain all the information about A that could be taken from the analysis of the Cherenkov light lateral distribution.

The estimates of the errors in determining A cited by the authors of the experiments in [1–6] are much lower than the scatter of the results (Fig. 1), which means, in our opinion, that one should review the existing methods and develop new ones with higher sensitivity to A and stability to the input parameters error.

The performed analysis shows that the mass composition of PCR can be determined using the correlations of the spatial–angular parameters of EAS CL with A without any intermediate stages of the measurement procedure.

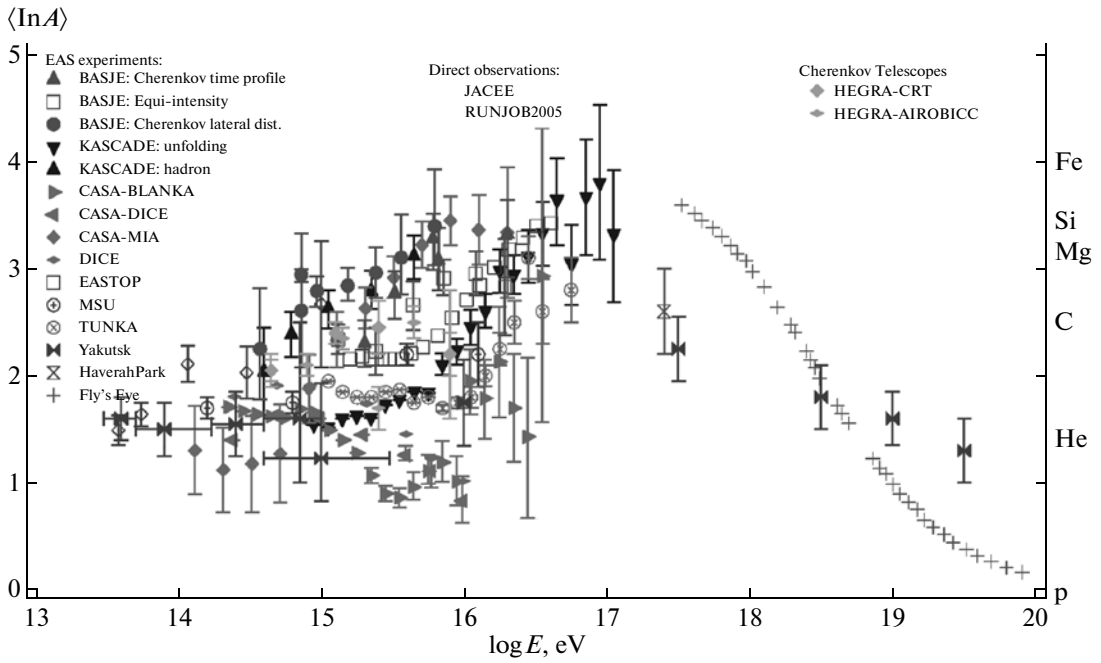

Fig. 1. Average logarithm of the mass of primary cosmic rays measured by different devices depending on the logarithm of the primary particle energy (adapted from [1]).

The spatial–angular distribution (SAD) of CL EAS, which is one of the most informative characteristics of an air shower, is quite sensitive to differences in the cascades determined by the type of the primary particle. One of the best-known confirmations of this thesis is the tremendous success of the Cherenkov γ-astronomy: a flow of γ-quanta of high energy from a point source is distinguished against the flows of cosmic ray nuclei exceeding the signal by 3–4 orders of magnitude [7–10]. There have already been some attempts to apply the method of Cherenkov γ-astronomy to the problem of investigating the mass composition of PCR in the primary energy range 1 TeV–1 PeV (e.g., [11, 12]). Here, the angular images are described using the traditional parameters of very high energy γ-astronomy: D (the angular distance from the source direction to the image's mass center), L (the mean-square semi-length of the image), W (the mean-square semi-width of the image), Conc (the image concentration, i.e., the ratio between the signal sum in the two maximum cells and the image's integral intensity), and the parameter H_{max} (the height of the radiation maximum) estimated by the image's mass center. The procedure for separating distinct nuclei groups based on this parameter set from the narrow-angle telescope data only (which does not allow accurate determination of other macroscopic parameters of the showers: the primary energy, direction, and core location) has demonstrated a moderate resolution capacity for A [12].

The present paper continues the investigation of the sensitivity of CL EAS characteristics to the mass composition started in [13–15]. The authors use detailed modeling to analyze the event separation criteria based on the traditional and newly determined parameters of the angular images and study the sensitivity of the latter to the mass A of the primary nuclei.

The purpose of this paper is to investigate the separability limits for PCR nuclei groups using EAS CL SAD, and it does not pose the problem of developing the specific configuration of a detector capable of using the found criteria. Section 1 describes the shower modeling procedure. Section 2 is dedicated to presenting the nuclei group separation procedure. Section 3 contains the results of classification using both traditional and new parameters. The possibilities of applying the proposed method are discussed in Section 4. Finally, in the Conclusions, the authors present the main conclusions of the present study.

1. MODELING

Using the CORSIKA 6.500 code [16] with QGSJET-II/GHEISHA nuclear interaction model [17, 18], a Cherenkov database of artificial EAS events has been obtained by means of full statistical modeling. The modeling procedure took account of the photodetector's quantum efficiency, which is consistent with the characteristics of the photomultiplier tube FEU-84-3 (the average over the spectrum ≈0.1, maximum ≈0.2 at a wavelength of ≈420 nm, and spectral sensitivity range of 310–655 nm). As a result of the modeling, four-dimensional histograms for photoelectron density were built; the histograms consist of 250 × 250 spatial

bins sized 2 × 2 m and 80 × 80 angular cells sized 0.5° × 0.5°. The axes of all the showers are at the center of the spatial part of the histogram; therefore, the histograms cover the distance range 0–250 m from the axis.

The space-time distribution was recorded separately; in each spatial bin, photoelectrons are distributed over 100 time intervals according to the time delay calculated from the moment of the arrival of the first relativistic particle to the observation level. The width of the time cell was 2 ns. The last, 101st, cell was an integral one; i.e., it contained all the optical photons with a time delay of more than 200 ns. Integrating the space–time distribution with respect to time produced a histogram of the so-called Cherenkov light spatial distribution function (CL SDF).

The classifiers presented below were obtained from the following event sample: for 1 PeV primary energy, 16 showers from primary protons and nitrogen nuclei when the observation plane was 1 km above sea level and 32 showers from similar particles for the height of 2 km above the sea level; for the 10 Pev energy level, showers from 16 protons and 16 nitrogen nuclei were used. In the latter case, the observation plane was at 1 km above sea level. Thus, a total of 128 model event were used. All the shower axes were vertical.

2. CONSTRUCTION OF THE CLASSIFIERS

To separate PCR nuclei groups, we used the so-called Bayesian approach with the assumption of a multi-dimensional normal distribution of the attributes [19]. The object classes in this case correspond to the types of the primary nuclei, with the learning sample being built from the model event base described in Section 1. Since only protons and nitrogen nuclei are considered, the number of classes $M = 2$.

At a considerable distance (~200 m) from the shower axis, the SAD of CL EAS $F(\theta_x, \theta_y)$ is essentially a highly oblong spindle-shaped spot of light (see Fig. 2), while, near the axis, the SAD has a less expressed asymmetry. This spot can be described with several parameters, for example, (D, L, W, Conc; see Introduction), with D and L increasing monotonously and W decreasing with the increasing distance from the axis. We analyzed the criteria for separating nitrogen nuclei and protons based on various combinations of these parameters measured simultaneously at several distances from the shower axis. Note that the image's second moments are quite sensitive to the behavior at the periphery of the SAD. On the other hand, the external part of the image is subject to the greatest signal fluctuations and background effects. Therefore, the values (D, L, W, Conc) were calculated using only those cells in which the signal value exceeded 100 photoelectrons.

Let us look at the CL angular image integrated over some region of the variable θ_y (i.e., over the horizontal band with the width $\delta\theta_y$ in Fig. 2, whose center matches that of the telescope's field of vision):

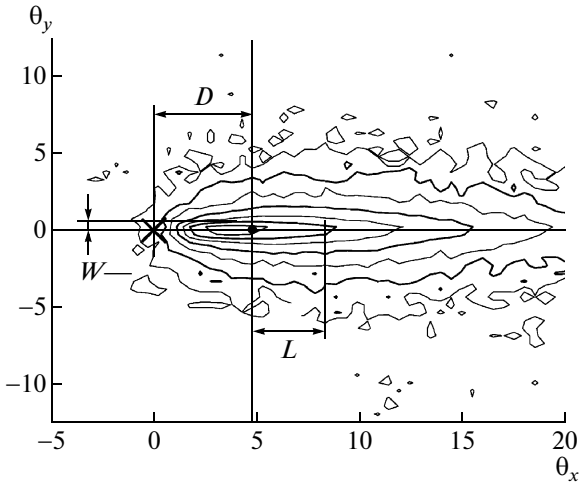

Fig. 2. Angular distribution of the Cherenkov light in a shower initiated by primary protons with energy 10 PeV at a distance of 200 m from the shower axis. The angles (θ_x, θ_y) (in deg) are plotted along the axes so that the center of the vision field (marked with a cross) corresponds to the zenith direction. The levels correspond to the isophotes of the signal intensity in the cells. The intensity logarithm corresponding to the external level is 0.5 and to the internal level is 3.5; the neighboring levels differ in intensity $\sqrt{10} \approx 3.16$ times. The mass center of the image is marked with a black circle. The figure also shows the segments corresponding to the parameters D, L, and W.

$$F_x(\theta_x) = \int_{-\theta_{y0}}^{\theta_{y0}} F(\theta_x, \theta_y) d\theta_y. \quad (1)$$

The physical meaning of the value $F_x(\theta_x)$ is the longitudinal angular distribution, or longitudinal profile of the angular distribution of the CL in the shower. Examples of longitudinal angular distributions of $F_x(\theta_x)$ are given in Fig. 3. Figure 3a shows $F_x(\theta_x)$ for several protons (gray curves) and nitrogen nuclei (black curves); Figure 3b presents the graph of the function $F_x(\theta_x)$ for different widths of the integration band $\theta_{y0} = 1.5°$ (black curve) and 20° (gray curve). The present paper investigates the criteria based on the use of the function $F_x(\theta_x)$ calculated with the value $\theta_{y0} = 1.5°$.

Let us introduce two new variables k and η:

$$k = \int_{\theta_{xk1}}^{\theta_{xk2}} F_x(\theta_x) d\theta_x \Big/ \int_{\theta_{xk3}}^{\theta_{xk4}} F_x(\theta_x) d\theta_x, \quad (2)$$

$$\eta = \int_{\theta_{x\eta1}}^{\theta_{x\eta2}} F_x(\theta_x) d\theta_x \Big/ \int_{\theta_{x\eta3}}^{\theta_{x\eta4}} F_x(\theta_x) d\theta_x, \quad (3)$$

where the integration limits are expressed in degrees and counted from the center of the telescope's field of view, and the function $F_x(\theta_x)$ is determined by formula

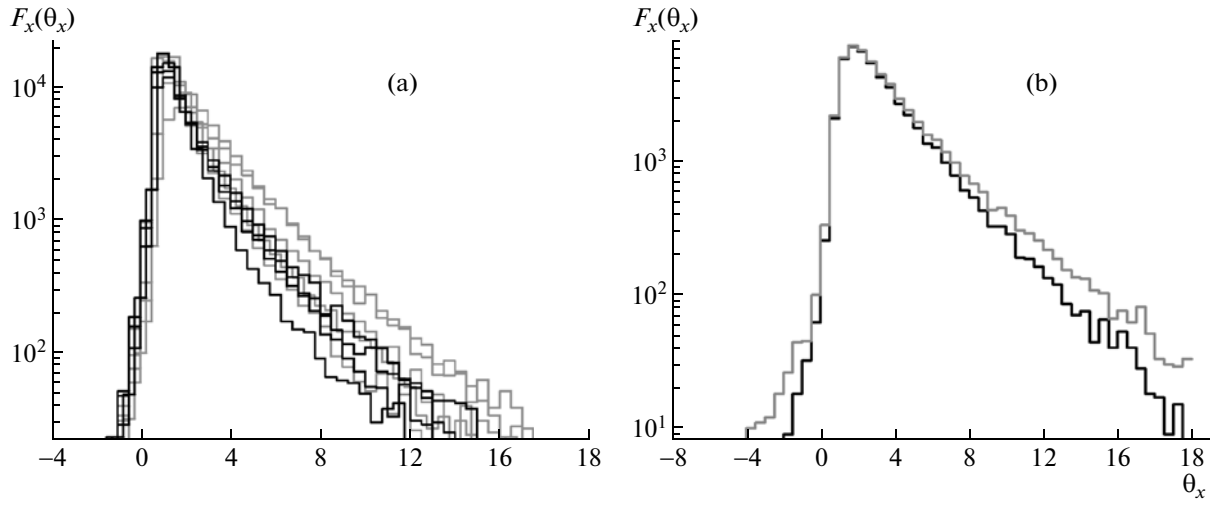

Fig. 3. (a) Longitudinal profile of the Cherenkov light $F_x(\theta_x)$ for several EAS at distance 100 m from the axis. The gray curves are the primary proton lines; the black, the nitrogen nuclei lines ($\theta_y = 1.5°$); (b) $F_x(\theta_x)$ of a shower initiated by a primary proton at different widths $\delta\theta_y$ of the integration band by θ_y 1.5° (black curve) and 20° (gray curve).

(1). The values of $\theta_{xk1} - \theta_{xk4}$ and $\theta_{x\eta1} - \theta_{x\eta4}$ were chosen in the present paper as follows: let the average maximum of the curve of the longitudinal angular distribution of the shower sample be located at some distance θ_{xM} from the center of the telescope's field of vision. The values θ_{xk1} and θ_{xk2} isolate a segment of the longitudinal angular distribution close to θ_{xM}. The values θ_{xk1} and θ_{xk2} limit a segment of the longitudinal angular distribution to the right of θ_{xM}, at some distance from this maximum. The value of the variable k for the showers initiated by primary protons is systematically greater than the one in the case of nitrogen nuclei. The values $\theta_{x\eta3}$ and $\theta_{x\eta4}$ isolate a segment on the curve close to the value θ_{xM}; $\theta_{x\eta1}$ and $\theta_{x\eta2}$, a segment before $\theta_{x\eta3}$. Both variables, k and η, demonstrate significantly greater fluctuations in the case of primary protons. The specific values of θ_{xk1}–θ_{xk4} and $\theta_{x\eta1}$–$\theta_{x\eta4}$ are given in the Results section. The variables k and η show good sensitivity to the type of primary nuclei, which is explained by well-known qualitative characteristics of the showers initiated by primary protons: they develop deeper in the atmosphere and are subject to the greatest fluctuations.

3. THE RESULTS OF THE CLASSIFICATION

As an example, let us consider the results of the classification using the parameters D and L calculated at distance 100 m from the shower axis. D and L are partially correlated; therefore, to get rid of most of the linear correlations, it would be convenient to introduce a new variable $L_c = L - (a_1 L + b_1)$. The values $a_1 = 0.98$ and $b_1 = 0.13$ are determined from the approximation of the dependence $L(D)$ for the proton-initiated showers with a linear function. Let $D_c = D$ so that the designations are symmetrical. Figure 4a presents the set of variables (D_c, L_c) for the case of the observation height of 1 km, $E_0 = 1$ PeV, and two types of primary nuclei. It is apparent that the use of the variables D_c and L_c does not ensure full separability of the classes of the primary proton and nitrogen nuclei.

Table 1. Errors of the multidimensional bayesian classification $E_0 = 1$ PeV, $H = 1$ km

N_p	Parameters	R, m	$\epsilon(p)$	$\epsilon(N)$
2	(D, L)	(100)	0.313	0.063
3	(D, L, W)	(100)	0.125	0.063
4	(D, L, W, Conc)	(100)	0.188	<0.063
8	(D, L, W, Conc)	(50, 100)	0.063	<0.063
12	(D, L, W, Conc)	(50, 100, 150)	<0.063	<0.063
16	(D, L, W, Conc)	(50, 100, 150, 200)	<0.063	<0.063

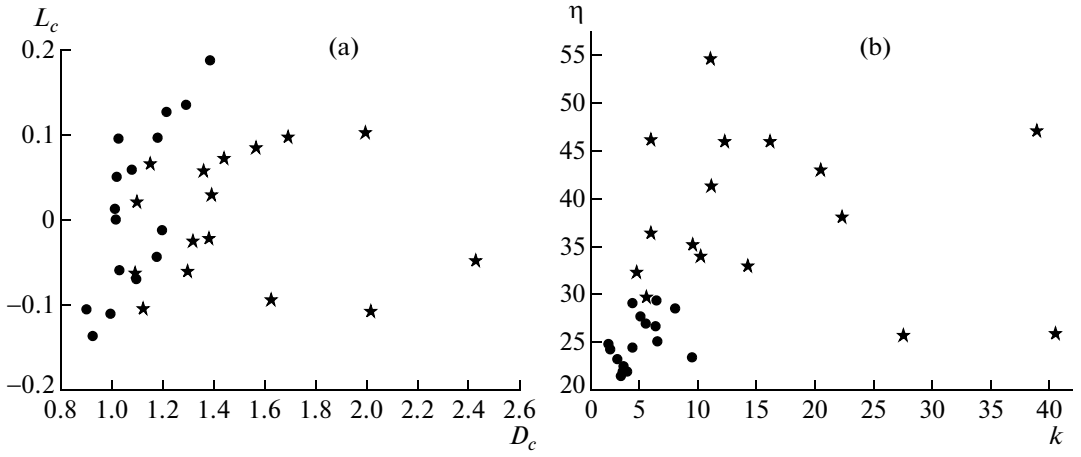

Fig. 4. (a) The plane of the variables (D_c and L_c) at a distance of 100 m from the axis. The stars denote the values of the variables corresponding to protons; the circles; nitrogen nuclei. $H = 1$ km, $E_0 = 1$ PeV; (b) the plane of the variables (k_c, η_c) was built under the same conditions as in Fig. 4a; $\theta_y = 1.5°$ (b).

Therefore, it would be more appropriate to use a classifier with a higher dimensional vector.

We investigated the dependence of the classification error for two types of nuclei on the set of variables in the attribute vector (see Tables 1–3). Table 1 presents these variables for the primary energy of 1 PeV and observation level of 1 km; Table 2, 1 PeV and 2 km; Table 3, 10 PeV and 1 km respectively. The first column in all these tables shows the number of parameters (dimensionality of the attribute vector). The second column lists the parameters as such; the third, the distances of the spatial distribution cells in which these parameters were calculated from the shower axis. The fourth column contains the classification error for protons ($\epsilon(p)$); the fifth, for nitrogen nuclei ($\epsilon(N)$).

Let us look at the data in Table 1. It is apparent that when we applying the criterion D, L with a two-dimension attribute vector, about 1/3 of the PCR primary protons are classified incorrectly. Inclusion of the variables W and Conc at the same point somewhat improves the situation, but the classification error for protons remains significant. On the other hand, the use of the spatial–angular distribution, i.e., the parameters D, L, W, and Conc at two or more distances from the shower axis allows one to correctly (accurate to the available statistics) classify all the nuclei.

The same dependence of the classification error on the number of variables can be seen in Table 2. The size of the learning sample used to build Table 2 is twice as large as the one used for Table 1. Therefore, one can clearly see from Table 2 that, even when using eight parameters (D and L at four distances from the shower axis), the errors of the classification procedure remains significant.

If the energy is increased from 1 to 10 PeV (Table 3), this does not worsen the separability of the nuclei. It is well known that the EAS development pattern is very weakly dependent on the energy; therefore, at medium energies 1 PeV $< E_0 <$ 10 PeV, the classifier properties based on the same variables as in Tables 1–3 should be expected to be close to those described above.

Now, let us pass to the classification results obtained using the parameters proposed in the present paper, i.e., k and η. Let us consider the case when the width of the integration band $\delta\theta_y = 1.5°$. Figure 4b shows the distribution of the same showers as in Fig. 4a, but with respect to the new variables (k, η). For convenience, the functions $F_x(\theta_x)$ were normalized by "the average function" for nitrogen nuclei, i.e., $\langle F_{xN}(\theta_x)\rangle$;

Table 2. Errors of the multidimensional bayesian classification $E_0 = 1$ PeV, $H = 2$ km

N_p	Parameters	R, m	$\epsilon(p)$	$\epsilon(N)$
8	(D, L)	(50, 100, 150, 200)	0.125	0.031
4	(D, L, W, Conc)	(50)	0.094	0.031
8	(D, L, W, Conc)	(50, 100)	0.063	<0.031
12	(D, L, W, Conc)	(50, 100, 150)	0.031	<0.031
16	(D, L, W, Conc)	(50, 100, 150, 200)	0.031	<0.031

Table 3. Errors of the multidimensional bayesian classification $E_0 = 10$ PeV, $H = 1$ km

N_p	Parameters	R, m	$\epsilon(p)$	$\epsilon(N)$
2	(D, L)	(50)	0.188	0.188
4	(D, L, W, Conc)	(50)	0.125	<0.063
8	(D, L, W, Conc)	(50, 100)	0.063	<0.063
12	(D, L, W, Conc)	(50, 100, 150)	<0.063	<0.063
16	(D, L, W, Conc)	(50, 100, 150, 200)	<0.063	<0.063

Table 4. Classification errors for the parameters k and η and different primary energies and observation heights

E_0, PeV	H, km	R, m	θ_{xk1}	θ_{xk2}	θ_{xk3}	θ_{xk4}	$\theta_{x\eta1}$	$\theta_{x\eta2}$	$\theta_{x\eta3}$	$\theta_{x\eta4}$	$\epsilon(p)$	$\epsilon(N)$
1	1	100	−0.5	1.0	1.5	6.0	−0.5	0.5	0.5	1.5	<0.063	<0.063
1	2	70	−0.5	2.0	3.0	8.0	−0.5	0.5	0.5	1.5	0.094	<0.031
10	1	100	−0.5	0.5	3.0	7.5	1.0	2.0	3.5	4.5	0.125	<0.063

then, we performed the calculations using formulae (2) and (3).

It is apparent that the use of the two new parameters greatly improved the separability of the classes of the primary protons and nitrogen nuclei as compared to the case of using (D_c, L_c). Thus, the showers initiated by primary protons and nitrogen nuclei can already be effectively separated when using only two parameters that are characteristics of the longitudinal profile of angular distribution of the CL EAS, i.e., $F_x(q_x)$.

The classification errors for the new parameters k and η are given in Table 4 (in this case, the number of parameters is fixed at 2). The first column of Table 4 presents the primary energy, the second column gives the height of the observation level; the third, the distance from the shower axis, the following eight values are the parameters in formulae (2) and (3), and the last two columns present the classification errors. The results of the multidimensional classification with the parameters k and η calculated at several different distances from the axis, as in the earlier case of using the variables D, L, W, and Conc, and the problems related to the optimal set of variables θ_{xk1}–θ_{xk4} and $\theta_{x\eta1}$–$\theta_{x\eta4}$, which were used to calculate k and η, are not discussed within the framework of the present paper.

The results obtained in the present paper are consistent with the properties of an angular telescope with a mirror diameter of 2 m, if one can neglect optical system aberrations and the distortions made by the electronic devices recording the CL. We also investigated the influence of the night sky background with the intensity of 3×10^{12} m^{-2} s^{-1} sr^{-1} and Poisson distribution on the classification error. The characteristic width of the timegate encompassing 90% of the integral with respect to CL pulse over time delay in each cell at distance < 200 m from the axis was found not to exceed 50 ns. Then, the Monte Carlo method was used to calculate the background fluctuations in each telescope cell during 50 ns, which were added to the effective signal (here, as in the case of the shower modeling, the photodetector quantum efficiency was taken into account). Finally, we ran the classification procedure using the input variables distorted by the presence of the background.

The following results refer to the case of the classification with 16 parameters, (D, L, W, Conc) taken at four distances from the shower axis: 50, 100, 150, and 200 m. The background was found not to affect the classification results at the energies of 1 and 10 PeV (i.e., the classification error was constant). This fact is explained by the high intensity of the signal in the central part of the angular distribution as compared to the background. Note that the signal–noise ratio in angular telescopes is much greater than in the typical angle integral detectors of the Cherenkov devices because the first type of detectors is selective by the angle and the stellar background is practically isotropic. Moreover, the angular Cherenkov telescopes have rather large mirrors (several square meters), which further improves the signal–noise ratio.

Furthermore, a tenfold increase of the background (i.e., to the level of 3×10^{13} m^{-2} s^{-1} sr^{-1}) was found to increase the classification error by 3–5%. Thus, the light background is important when performing measurements in conditions of increased clutter (e.g., from the Moon) and the classification procedure at lower energies of the primary particle, i.e., ~100 TeV.

Finally, the developed criteria were tested for their stability to the calibration errors of particular pixels of

the telescope. For this purpose, for each δ = (0.01, 0.03, and 0.05), we simulated out a sample of 100 matrices of the pixels calibration coefficients as follows: each of the $80 \times 80 = 6400$ elements of the matrix was assigned the calibration coefficient $1 + \delta$ or $1 - \delta$ with an equal probability. Each of the matrices was then used to modify the artificial images of the showers of both the classes under study (protons and nitrogen nuclei); the content of each pixel was multiplied by the respective calibration coefficient. Then, the modified images were classified using the criterion constructed under the ideal calibration assumption. This was followed by building the distribution of the increments $\Delta\epsilon(p)$ and $\Delta\epsilon(N)$ to the classification errors $\epsilon(p)$ and $\epsilon(N)$ caused by the calibration errors of the telescope pixels. In the case of the energy of 1 PeV and position of the observation level at 2 km, the average values of these increments were: $\Delta\epsilon(p) = 8.0\%$ and $\Delta\epsilon(N) = 1.8\%$ at $\delta = 0.05$, $\Delta\epsilon(p) = 3.9\%$ and $\Delta\epsilon(N) = 1.2\%$ at $\delta = 0.03$, and $\Delta\epsilon(p) = 0.5\%$ and $\Delta\epsilon(N) = 0.1\%$ at $\delta = 0.01$.

4. APPLICATION OF THE DEVELOPED CRITERIA

The described criteria depend on the parameters of the EAS angular images recorded by wide-angle optical telescopes located at various distances from the shower axis. In the present paper, these distances were fixed. However, an angle integral detector grid with a step < 100 m is known to provide measurements of the shower axis position with an error of $\delta R \sim 5$ m; therefore, the method applied in the present paper can be generalized for the case of an arbitrary position of the shower axis with respect to the detectors. For the application of the criteria to separate the PCR nuclei groups to be successful one should also know the direction of the shower arrival with high accuracy: $\delta\theta \sim 0.1^\circ$. The measurements of the spectra of various nuclei groups also imply that the energy be measured with an accuracy of $\delta E_0 \sim 15\%$. Even several angular telescopes cannot ensure the necessary precision of determining the core location, primary energy, and direction. Therefore, to implement the spatial–angular Cherenkov selection criteria for the mass of the primary particle, one needs, in addition to several wide-angled optical Cherenkov telescopes, a set of fast wide-angled optical detectors with the sensitive area of ~1 m^2 and a temporal resolution of ~2 ns that create a regular (rectangular or hexangular) grid with a step of ~30 m. Locating 3–4 angular telescopes at ~100 m from one another in the central part of this grid allows one to obtain very detailed data on each recorded shower so that one can use the properties of CL SAD to analyze the mass composition of PCR. The fairly dense grid of angle integral detectors allow one, apart from determining the core location, primary energy, and direction of the shower arrival, to measure the lateral distribution of the CL, which is also sensitive to the mass of the primary nucleus [13–15].

CONCLUSIONS

Full statistical modeling of the spatial–angular distribution of the Cherenkov light in extensive air showers (EAS CL SAD) is used to build two families of criteria to separate the showers initiated by protons and nitrogen nuclei of primary cosmic rays (PCR) with energies of 1–10 PeV. The criteria are built using the method of multi-dimensional Bayesian classification under the assumption of a normal distribution of the attributes. The classification errors for these groups of primary nuclei are shown to be a few percent (≈3% in the case of the observation level at 2 km and primary energy of 1 PeV). Apart from the criteria based on the variables D, L, W, and Conc (see Introduction), the new parameters k and η are proposed; these parameters allow one to greatly increase the separability of the primary nuclei classes and simplify the classification procedure. The variables k and η have the physical meaning of the asymmetry and "slope" of the longitudinal profile of the angular distribution of CL EAS.

The developed criteria can be used to investigate the mass composition of primary cosmic rays within the indicated energy interval, where a knee is observed in the PCR spectrum. The discussed method has a high probability of successful application, both at lower (<1 PeV, in the case of increased telescope mirror) and higher energies (>10 PeV, in the case of an increased effective geometric factor of the detector array by increasing the area occupied by the array or the solid angle observed by the photomultiplier tube matrix in the focal surface of the telescope mirror).

ACKNOWLEDGEMENTS

This work was supported by the Federal Agency for Science and Innovations, government contract no. 02.740.11.5092, and Program for Leading Scientific Schools Support (project NSh-959.2008.2).

REFERENCES

1. Y. Tsunesada, F. Kakimoto, F. Furuhata, et al. (The BASJE Collab.), Proc. 30th ICRC (Merida) **4**, 127 (2008).
2. T. Antoni, W. D. Apel, A. F. Badea, et al. (The KASKADE Collab.), Astropart. Phys. **24**, 1 (2005).
3. M. Aglietta, B. Alessandro, P. Antonioli, et al. (The EAS-TOP Collab.), Astropart. Phys. **21**, 583 (2004).
4. J. W. Fowler, L. F. Fortson, C. C. H. Jui, et al., Astropart. Phys. **15**, 49 (2001).
5. F. Arqueros, J. A. Barrio, K. Bernlohr, et al. (The HEGRA Collab.), Astron. Astrophys. **359**, 682 (2000).
6. D. V. Chernov, E. E. Korosteleva, L. A. Kuzmichev, et al. (The Tunka Collab.), Int. J. Mod. Phys. A **20**, 6799 (2005).

7. T. C. Weekes, M. F. Cawley, D. J. Fegan, et al., Astrophys. J. **342**, 379 (1989).
8. G. Puhlhofer, O. Bolz, N. Gotting, et al. (The HEGRA Collab.), Astropart. Phys., 267 (2003).
9. J. A. Hinton, New Astron. Rev. **48**, 331 (2004).
10. D. Ferenc (for the MAGIC Collab.), Nucl. Instrum. Methods Phys. Res. A **553**, 274 (2005).
11. A. V. Plyasheshnikov, A. K. Konopelko, F. A. Aharonian, et al., J. Phys. G **24**, 653 (1998).
12. F. A. Aharonian, V. V. Bugayov, J. Kettler, et al., Nucl. Instrum. Methods Phys. Res. B **201**, 217 (2003).
13. A. M. Anokhina, R. A. Antonov, E. A. Bonvech, et al., Proc. 30th ICRC (Merida) **5**, 945 (2008).
14. A. M. Anokhina, R. A. Antonov, E. A. Bonvech, et al., Bull. Lebedev Phys. Inst. **36**, 146 (2009).
15. A. M. Antonov, A. M. Anokhina, E. A. Bonvech, et al., Proc. 31th ICRC (Lodz, 2009), ID 434.
16. D. Heck, J. Knapp, J. N. Capdevielle, et al., Forschungszentrum Karlsruhe Rep. FZKA 6019 (1998).
17. S. Ostapchenko, Nucl. Phys. Proc. Suppl. B **151**, 143 (2006).
18. H. C. Fesefeldt, Techn. Report PITHA 85–02 (RWTH, 1985).
19. S. Theodoridis and K. Koutroumbas, *Pattern Recognition* (Elsevier, San Diego, 2003).